UNIVERSITÀ DEGLI STUDI DI PADOVA

Dipartimento di Fisica e Astronomia "Galileo Galilei"

Corso di Laurea in Fisica

Tesi di Laurea

Connettività dinamica e non-linearità in un modello computazionale del cervello

Dynamical connectivity and nonlinearity in a whole-brain computational model

Relatore

Prof. Michele Allegra

Laureando

Paolo Lapo Cerni

Anno Accademico 2022/2023

Abstract

Among the large variety of models for large-scale brain activity, effective models achieve a good trade-off between model accuracy and complexity and can be fit to activity data of individual subjects from functional magnetic resonance imaging. We will use an effective model of whole-brain dynamics to fit individual brain activity data from the Human Connectome Project (a large neuroimaging database) and address the relationship between the model nonlinearity and the "dynamic functional connectivity" (temporal variations in the correlation between signals of different areas). In particular, we will focus on the "dynamic functional connectivity speed", a scalar index measuring the rapidity of variation in connectivity patterns, and investigate whether the model reproduces its empirical distribution and whether the latter is related to the model's nonlinearity.

*Tra la grande varietà di modelli per l'attività cerebrale su larga scala, gli "*effective models*" raggiungono un buon compromesso tra accuratezza e complessità del modello e possono essere adattati ai dati di risonanza magnetica funzionale dell'attività dei singoli soggetti. Useremo un modello delle dinamiche del cervello per analizzare i dati dell'attività cerebrale individuale dal Progetto Human Connectome (un grande database di neuroimaging) e affronteremo la relazione tra la non linearità del modello e la "connettività funzionale dinamica" (variazioni temporali nella correlazione tra i segnali di aree diverse). In particolare, ci concentreremo sulla "velocità di connettività funzionale dinamica", un indice scalare che misura la rapidità di variazione nei modelli di connettività, e indagheremo se il modello riproduce la sua distribuzione empirica e se quest'ultima è correlata alla non linearità del modello.*

Contents

Chapter 1

Introduction

1.1 Dynamics of brain activity

Understanding the complexity of brain activity, even during the resting state, is an open challenge in neuroscience. Large-scale brain activity can be studied by looking at correlations in blood oxygenation-level dependent (BOLD) signals across different brain regions, which have been shown to exhibit nontrivial patterns and structured temporal variability [1]. During the last two decades, studies emphasized that fluctuations in these signals have neurophysiological origins and contain information about the macro-scale spatiotemporal organization of the brain [1, 2].

To investigate these mechanisms it is common to study the functional connectivity (FC) of functional magnetic resonance imaging (fMRI), usually during resting state when there are no other contributions except for the spontaneous dynamics. The FC is defined as the *temporal coincidence of spatially distant neurophysiological events* (Friston, 1994) so it measures the statistical relationship between two brain regional time courses, typically (but not always) by Pearson correlation. It follows that FC measures are *static* because they average signals over a certain period. Given an atlas of the brain regions and the corresponding rs-fMRI time series, the entries of the *FC matrix* contain the correlation between any pair of time series (BOLD signals). Note that while *structural connectivity* emphasizes the existence of an anatomical connection between neuronal regions, FC refers to time coordination in activity.

The complexity of brain activity suggests that there might be some information beyond the static FC. The focus of recent research so has shifted from the analysis of the FC averaged over the entire scanning sessions to the analysis of changes in the FC within the same session. This approach allows researchers to investigate temporal FC variability, also called dynamic functional connectivity (dFC). To interrogate dFC is common to use the sliding windows correlation (SWC) analysis. This method consists of sampling time-dependent FCs from the rs-fMRI time series by sliding a temporal window of fixed duration and with fixed overlap between successive windows. This approach leads to a sequence of time-resolved FC matrices, called *dFC stream*. Changes in brain organization, emerging from FC fluctuations, can be interpreted as the result of a stochastic exploration of a high-dimensional space. To quantify the FC variability it is therefore necessary to define a metric of similarity between two FC matrices and analyze its variation over time. This could be again done with some measure of correlation.

Generative models are another tool to better understand brain dynamics. They provide a formal mathematical description of the time evolution of brain activity that can be used to generate surrogate time series to compare with the actual data. There are several approaches to define these models, based on either biological observation or data-driven statistical characterization. Some of these approaches work in linear approximation, while others are inherently nonlinear and dynamic. The aim of these analyses is to reproduce some features of the actual data (such as the FC or the dFC speed) and study what are the dynamical mechanisms underlying the observed, complex brain activity time series.

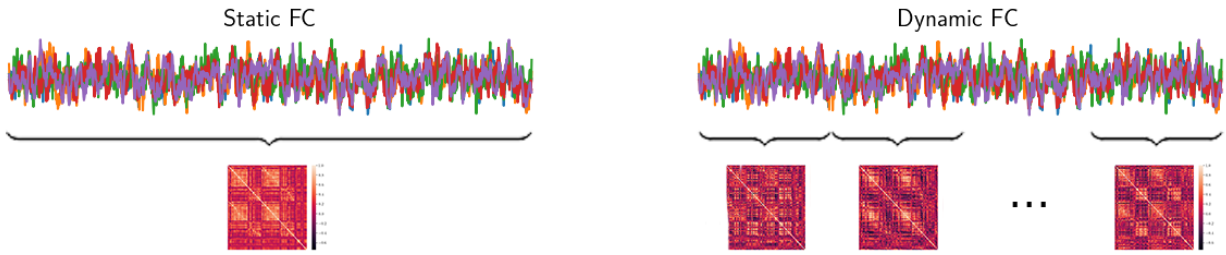

Figure 1.1: Comparison between static and dynamic functional connectivity matrices. On the left, the static case is obtained from the full scan time series. On the right, the dFC stream from the SWC analysis.

Used abbreviations

In order to achieve a more readable text, several technical terms will be used with abbreviations. The following table 1.1 provides a comprehensive overview of the abbreviations used.

Abbreviation	**Meaning**
rs	resting state
fMRI	functional magnetic resonance imaging
BOLD	blood oxygenation-level dependent
FC	functional connectivity
dFC	dynamic functional connectivity
TR	repetition time
SWC	sliding window correlations
HCP	Human Connectome Project

Table 1.1: List of Abbreviations

1.2 Issues in testing dFC

It is not trivial to understand whether fluctuations in functional connectivity reflect actual dynamic changes in brain organization or just some type of noise.
It is crucial to explicitly define some terminology: "static" vs. "dynamic" and "time-varying" vs. "time-invariant", because a loose use of these terms contributes to possible confusion [3]. The terms *static* and *dynamic* refer to whether or not the model or the measures are invariant to the temporal re-ordering of data points. For example, Pearson's correlation coefficients between times series of the entire fMRI session are static, because permuting the order of some frames won't change the results. In this term, standard functional connectivity is a static measure of the temporal coincidence between activities in neural populations. On the other hand, dFC is inherently dynamic because the sliding windows correlation analysis is not invariant to the re-ordering of data points.
If some parameters of the model, or some measures, are explicitly functions of time, they are called *time-varying* or *non-stationary*. If they are invariant to time translations they are called *time-invariant* or *stationary*. While being dynamic, dFC is not necessarily time-varying.

Assessing stationarity of fMRI time series is problematic, because this property is well-defined in the framework of *ensemble statistics*, and therefore requires multiple realizations of the same random process to be estimated. However, fMRI data from a multi-subjects dataset are typically considered single realizations of different random processes, one for each subject (*sample statistics*). Ideally, we would like to have access to multiple parallel sessions of the same fMRI scan for the same individual. Instead, we have single scans from multiple subjects, which represent different random processes to deal with. While we would be tempted to assume the equivalence of ensemble and sample statics

(*ergodicity*), ergodic processes are by definition stationary so this assumption would jeopardize the attempt of studying the stationarity/non-stationarity of the system.

Related to this, the mere presence of fluctuation in the FC time series is not even evidence of non-stationarity. In fact, a large part of the observed variation might be explained by sampling variability [4], and also vigilance, arousal, and emotions could interfere with the study of fMRI data [5]. Thus, at least a part of the observed dynamic could be due to accidental conditions or experimental uncertainties.
Furthermore, stationarity does not imply the absence of distinct brain states (clusters of similar network configurations in the brain organization) or variability in FC data while there are processes, such as hidden Markov processes, which exhibit transitions between discrete states despite their being stationary [3].
So, temporal fluctuation does not directly imply the necessity of non-stationary dynamical models.

A typical approach to test stationarity is to generate null data from a procedure that preserves specific properties of fMRI realizations but that assumes stationarity. Statistically significant deviations of the real data from the surrogate time series would result in the rejection of the hypothesis of stationarity. The test procedure should reflect the null hypothesis without introducing any other constraint to the model. However, the standard techniques cannot test stationarity alone and a rejection of the null hypothesis only implies non-stationarity or non-linearity or non-Gaussian, or any combination of the above [3].

As described in the paragraphs above, there are several technical and fundamental issues in testing dynamical functional connectivity. However, recent researches emphasize how the dynamical and non-linear characterization of the fMRI sessions can successfully provide some useful tools to understand the underlying phenomena. Thus, despite the critical aspects, studying the dynamic of brain activities is an open and florid topic in computational neuroscience.

1.3 Data and preprossessing

We used the 96 unrelated subjects' subset from the Human Connectome Project (HCP) [6].
For the main analysis, we used the left-right (LR) phase-encoding runs from the first session resting state fMRI data. We later replicated the analysis for the left-right (LR) phase-encoding runs from the second session resting state fMRI data.
Recordings had ≈ 15 min duration with a TR of 0.72 sec. The full description of the imaging parameters and minimal preprocessing pipeline is given in Ref. [7]. In short, after correction for motion, gradient, and susceptibility distortions the fMRI data was aligned to an anatomical image. The aligned functional image was corrected for intensity bias, demeaned, and projected to a common surface space, which resulted in a cifti-file. All fMRI data were filtered between 0.1 and 0.01 Hz to retain the relevant frequency range for further analyses of the BOLD signal.
We obtain structural and functional matrices in different spatial scales using the Schaefer parcellation [8], which optimizes local gradient and global similarity measures of the fMRI signal in various spatial scales. We considered the spatial scale corresponding to 100 regions. In both fMRI datasets time series were extracted with the help Workbench Command provided by the HCP.
In addition, we considered 19 subcortical regions derived from the FreeSurfer subcortical atlas [9, 10].

Chapter 2

Methods and analysis

2.1 Dynamic functional connectivity

Brain states are operationally described as similar configurations in terms of functional connections between regions. They can be thought of as clusters in the abstract high-dimensional space of the possible arrangements. Even if statistical evidence for the non-stationarity of the resting state FC or the actual existence of discrete and distinct FC states is not conclusive, there is growing evidence that treating FC as not static but inherently dynamic can be used to develop sensitive biomarkers of the efficiency and flexibility of cognitive processing. Moreover, dynamic approaches can be used to characterize pathological alterations or differences between different subjects.

dFC streams

In the context of studying FC dynamics, there is no consensus on whether fluctuations in FC resemble isolated transitions between discrete states rather than continuous changes. Battaglia et al. [11] tried to merge these two perspectives considering dFC as the result of a smooth flow across continually morphing connectivity configurations. This approach may explain deviation both from purely "order-driven" dynamics and from a purely "randomness-driven" scenario.
Conventional analysis on static FC emphasized the spatial structure of neural networks, losing information about the time evolution of functional connections and the potential manifestation of some type of collective emergent dynamics. The proposed approach is the opposite: by evaluating features obtained from dFC, space is de-emphasized in favor of time. FC networks collapse to a point in the high-dimensional space of FC possible configurations and their evolution can be interpreted as a random walk in that space. Fluctuations are treated as the result of ongoing network reconfiguration, which includes some stochastic exploration of the space of possible steady FC states.

In order to develop quantitative tools to investigate this stochastic walk, we need to define some attributes of our resting-state BOLD time series (TS) data.
Firstly, we need to quantify the agreement between different signals from different brain regions. This can be done with time-averaged functional connectivity matrices. Each matrix entry contains the correlation between time series from different brain regions i and j in a temporal window of fixed duration τ.

$$\mathrm{FC}_{ij}(t) = \mathrm{Corr}[\mathrm{TS}_i(t'), \mathrm{TS}_j(t')] \quad \text{over} \quad t - \frac{\tau}{2} \leq t' \leq t + \frac{\tau}{2}$$

Correlation is quantified with the zero-lag Pearson coefficient defined in terms of two random variables (X, Y) as follows:

$$\mathrm{Corr}(X, Y) = \frac{\mathbb{E}[XY] - \mathbb{E}[X]\mathbb{E}[Y]}{\sqrt{\mathbb{E}\left[X^2\right] - (\mathbb{E}[X])^2}\sqrt{\mathbb{E}\left[Y^2\right] - (\mathbb{E}[Y])^2}}$$

where $\mathbb{E}[X]$ indicate the expectation values of X. It is the covariance of (X, Y) normalized for their standard deviations and quantifies the linear correlation between them.
In the FC matrix, no statistical test is used to assess the significance of single links.

These correlation matrices are of course symmetric, so a FC state can be identified with the vector containing the values of the upper triangular matrix. Note that these states depend on the hyperparameter τ, which tunes the loss of information about dynamical changes in FC.

According to Battaglia et al. [11], we will refer to the sequence of time-dependent FC matrices as *dFC stream*. These streams are obtained by sliding a temporal window of size $W = \tau$ with no overlap between contiguous windows (sliding windows correlation, *SWC*).

To evaluate transitions between FC states, we need a metric to quantify the similarity between FC frames observed at different times. The so-called *dFC* is defined as the plain correlation between the upper triangular parts of two FC matrices.

$$\mathrm{dFC}(t_1, t_2) = \mathrm{Corr}[\mathrm{UpperTri}(\mathrm{FC}(t_1)), \mathrm{UpperTri}(\mathrm{FC}(t_2))]$$

The correlation is again based on the Pearson coefficient, however, it would be possible to redefine this metric with more sophisticated statistical tools.

A visualization of the temporal structure of the similarity between FC(t) networks can be provided into a *dFC matrix*, a recurrence matrix whose entries (i, j) report the $dFC(t_i, t_j)$. These matrices usually show characteristic patterns composed of square-shaped blocks that reflect the inhomogeneous speed of variability along the single dFC stream.
These provide a visual tool to understand the stochastic walk across epochs of relative FC stability, where are displayed sequentially correlated short jumps, and random explorations of other possible configurations.

Global dFC speed

For quantitative analysis of rates of FC variation over time, it is necessary to measure the amount of change between two FC observations separated by a fixed amount of time. We thus define the *instantaneous global speed* as:

$$V(t) = 1 - \mathrm{dFC}(t, t + \tau)$$

This metric measures the correlation distance between two contiguous FC matrices in a dFC stream. The term "instantaneous" refers to the fact that the two observations are separated by an amount of time set to be equal to the window size W, so they are contiguous in the stream. Moreover, the speed is termed "global" because it is evaluated by comparing the whole-brain FC upper triangular matrices.

Once again, dFC speed depends on the chosen τ. fMRI sessions generally yield short time series ($\sim$ 10-15 minutes), and if sliding windows are long (large τ) the number of independent measurements of V is small. A strategy to increase the statistics by increasing the number of sampled speed observations and avoid potential aliasing is *window pooling*. The key idea is that distributions obtained with close enough τ are very similar and largely overlapped, if not statistically indistinguishable. It is therefore reasonable to re-sample dFC speed with values of τ' close to τ and merge the histograms to achieve larger samples. Not only does this lead to smoother histograms, but it also allows the severity of the multiple-comparisons correction (which is more severe for small samples) and it blurs possible spurious anomalies from artefactual aliasing due to the use of a single window length [12, 13].

From histograms of dFC speed one can extract various features of interest that can characterize different subjects or groups of subjects. For example, the position of their mode can be thought of as a measure of the typical speed of re-configurations across FC states and can provide a first indicator of the expected scale of time for network variability along the dFC stream. Moreover, some measures of dispersion can be useful to understand the behavior of the stochastic exploration of the high-dimensional space of configurations.

The dFC speed has been shown to highlight group differences when computed for different groups of subjects. For example, the medians of the distributions correlate negatively with the ages of healthy subjects over a broad range of window sizes [11]. This shows the slowing of dFC through the human

adult lifespan that may be linked to a general reduction of FC(t) variance, possibly interpreted as the fact that aging leads to replacing network complexity with randomness in the stochastic exploration of possible configurations.
This metric also correlates positively with task and cognitive performance, e.g., in simple visuomotor tasks. Thus, V yields relevant information not only during the resting state, but also task states [11]. Moreover, dFC speed can also differentiate subjects with sleep deprivation, treated as a reversible model of cognitive dysfunction [14]. The typical global speed of reconfiguration during the resting state is significantly slower after sleep deprivation. However, it is not possible to predict small and specific changes in cognitive performance caused by this type of condition because they are moderate and diverse for different tasks. More detailed analysis can be done by introducing the so-called *modular dFC speed* which allows to quantify rates of fluctuation for each different sub-network of interest. Performing separate analyses for each module can emphasize correlations between changes in speed after sleep deprivation and cognitive performance in specific tasks.

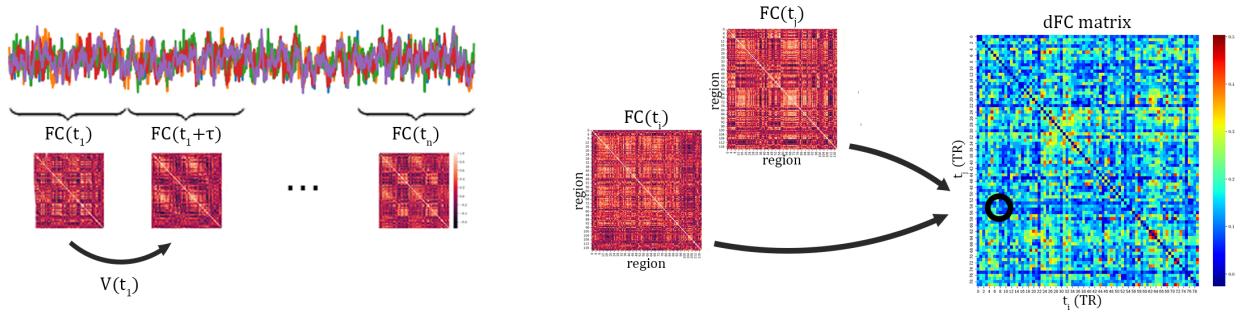

Figure 2.1: On the left, the stream of time-resolved FC matrices (dFC stream) obtained by the SWC analysis with window τ. The dFC speed $V(t)$ quantifies the amount of change between contiguous FC realizations. On the right, the entries of the dFC matrix report the correlation between pairs of FC states.

2.2 MINDy model

Generative causal models can provide a mathematical description of how the activity of the human nervous system evolves in time, in terms of spatial and temporal connections between neural structures. It is an open challenge in the field of computational neuroscience due to the complexity of the system.

Standard approaches can be summarized in two main categories. Firstly, there are generative models developed by integrating cellular-level observations with a biologically-plausible mechanistic model. They are based on biophysical studies of small populations of neurons but they often fail to reproduce individual-level human brain activities. On the other hand, there are data-driven models aiming at a precise statistical characterization of individual subjects. Typically, they focus on correlations between activity signals, trying to reproduce higher-level statistical summaries, such as static functional connectivity. As a result, they are not mechanistic and they might be unable to fully capture the complexity of brain activity.
Singh et al. [15] tried to merge these perspectives in a nonlinear dynamical model fitted directly to human brain imaging data. This new modeling approach is called *Mesoscale Individualized Neurodynamic* (MINDy).

Description of the model

The MINDy model consists in the mathematical description of connections between hundreds of interacting neural populations and it reproduces the evolution of brain dynamics over time scales commensurate with fMRI observations, with which the model is trained. This approach provides an efficient data-driven fitting procedure with biologically interpretable parameters.
The typical connectivity matrix of rsFC has been expanded to a powerful dynamical model for the

activity of each region:

$$\dot{x} = W\psi_\alpha(x_t) - Dx_t + \varepsilon_t$$

Where ψ_α is the sigmoid-shaped transfer function defined as:

$$\psi_\alpha(x_t) = \sqrt{\alpha^2 + (bx_t + 0.5)^2} - \sqrt{\alpha^2 + (bx_t - 0.5)^2}$$

This model is inherently phenomenological and is not directly derived from biophysical first principles. However, this fact does not preclude the interpretability of its components and parameters [16].

x_t: the time-dependent vector storing the brain activity at each anatomical location, according to the given atlas of the regions of the nervous system.

W: the weight matrix of connections between neural populations that tunes the causal ability of the mean activity of region A to change the mean activity of region B monotonically. Thus, increasing (decreasing) the activity in A will never decrease (increase) the activity of region B. To be captured, the causal effects of an interaction must have a temporal range between 500ms and 2s, beginning within the duration of one TR (typically $\sim$ 1s) and last long enough to evoke an observable metabolic response.
Thus, this matrix describes the effective connectivity rather than the structural one.

ψ_α: the sigmoidal transfer function that describes the local activity of a neural population and its relationship with other regions. Although it has to be treated as a phenomenological function, it could be linked to the probability of neural spiking as a function of excitatory stimuli. Higher values of its slope may depend on both greater heterogeneities in responses within the population and greater synchronization of excitatory external inputs.
It is tuned by the fixed global hyperparameter b (set to be $b = 20/3$) and by α. The latter is fitted on a subject-wise basis and it is specific for each brain region. It parameterizes the shape of the curve and the (non)linearity of the responses. Greater values of this parameter correspond to greater linearity in responses to stimuli.

D: the diagonal decay matrix whose terms describe how quickly the activity of each population returns to its baseline value. Without considering any other effects or external inputs, the time course will be exponential. However, this hypothesis is relaxed by the fact that "self-connections" are allowed in the connectivity matrix W. The competing nonlinear self-excitation and the linear self-inhibition lead to a richer spectrum of possible dynamics at the population level.

ε_t: the process noise, which is assumed to be uncorrelated between parcels. We used a Gaussian unbiased noise, whose role in dynamics and performances will be investigated.

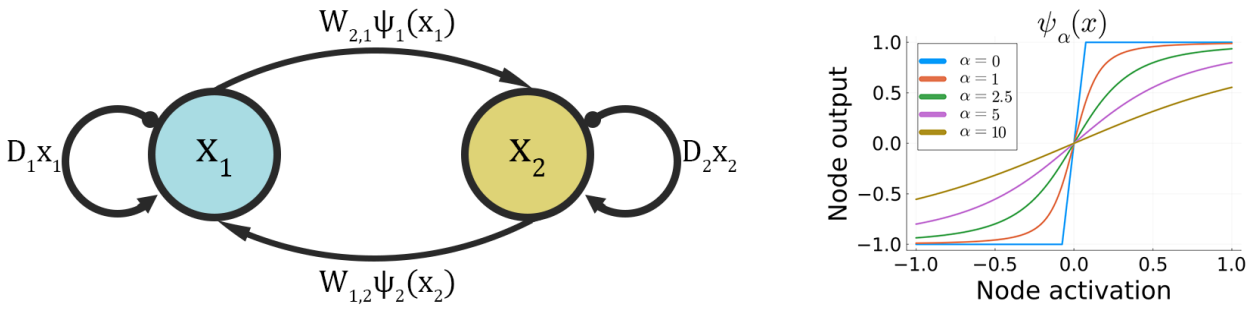

Figure 2.2: On the left, the MINDy schema about the interaction between two different neural populations. The correspondent elements of the weight matrix tune the correlation between the parcels. On the right, the shape of the sigmoidal transfer function and the relationship between α and the non-linearity of the response.

Both for the fitting procedure and the time series prediction it is necessary to approximate the neural model with a time discretization tuned by a temporal resolution Δt (related to the sampling TR).

The explicit Euler's method for numerical integration of ordinary differential equations has been used as follows:

$$x_{t+\Delta t} = x_t + (W\psi_\alpha(x_t) - Dx_t + \varepsilon_t)\Delta t$$

Training and inference

The fitting procedure is beyond the purpose of this work, but it is nevertheless important to emphasize some of its aspects [16]. The model is fitted by a variant of the stochastic gradient descent, NADAM (Nesterov-accelerated Adaptive Moment Estimation), which combines the computational efficiency of classical optimization methods and the ability to handle non-convex surfaces in the space of parameters. NADAM uses a "momentum" term in the update rule to make the system's evolution a function of past gradients too. Thus, together with the parameters, this algorithm evaluates the moving average of both the gradient and the squared gradient and uses them to prevent over-fitting and improve cross-validation at each step.
NADAM involves four hyperparameters: the learning rate of the update rule, two decay terms for the moving averages, and one regularization parameter to stabilize the learning rate and prevent division by zero.

The connectivity matrix W is decomposed into two terms: one $n \times n$ sparse component W_S and a low-dimensional matrix $W_L = W_1 W_2^T$ in which both W_1 and W_2 are $n \times m$ rectangular matrices, where n is the number of neural populations and $m < n$ denotes the chosen dimensionality of the diffuse matrix. Hence, $W = W_S + W_L$.

The chosen loss of the minimization problem, including the regularization terms, is defined as:

$$J = \frac{1}{2}\mathbb{E}_T[||(X_{T+\Delta t} - X_T) - [(W_S + W_L)\psi_\alpha(X_T) - DX_T]||_2^2] +$$
$$+\lambda_1||W_S||_1 + \lambda_2 \mathrm{Tr}(|W_S|) + \lambda_3(||W_1||_1 + ||W_2||_1) + \frac{1}{2}\lambda_4||W_L||_2^2$$

The notation $\mathbb{E}_T$ denotes the expected value over all time points within the minibatch of each iteration, so the first term corresponds to the mean square error of predictions. The sparsity of W_S is achieved with the L_1 regularization penalty depending on the global constant λ_1. Also both the diffuse components are L_1 penalized with the same coefficient λ_3. The combined W_L matrix also receives L_2 penalization. The four regularization terms λ_i are shared across all subjects and are the most impactful hyperparameters of the model.

MATLAB code and some documentation for the MINDy model are available via Matthew F. Singh's GitHub page. In particular, we used the high-level function *MINDy_Simple* which only needs the parcellated time-series data as training inputs. In terms of phenomenological significance, the returned relevant parameters are the weights W, the curvature α, and the decay term D.

Performance of the model

Singh et al. [15] studied the performance of the MINDy model, whose most important aspects will be described in the following paragraphs.

The model is sufficiently sensitive to retrieve individual differences between subjects in terms of connectivity weights. This has been tested by comparing the weights matrix and the simulated functional connectivity across different patients. MINDy is able to simulate weight changes that differentiate individuals and produce accurate rsFC. Furthermore, it has been proved that the goodness of both single time-step prediction and simulated FC significantly increases when evaluated within the same subject rather than across different subjects.

The model fitting procedure is also empirically reliable. This aspect was tested by the repetition of the fMRI scans on two separate days and by measuring the test-retest reliability of the estimated parameters. So MINDy parameters are both personalized and reliable.

The MINDy model is also been proved robust to the three main sources of measurement noise. Shortly, it is robust to noise in the BOLD signals (which is also related to the patient's motion during the scan session), to post-processing pipelines that attempt to mitigate the noise, and to variation in the used estimation of the hemodynamic response function.

Chapter 3

Results and discussion

3.1 Global speed ground truth

The global dFC speed provides a powerful tool to investigate the similarity between contiguous realizations within a dFC stream. It is a measure of the speed in the brain activity reconfiguration within a scan session. Its distribution depends on the hyperparameter τ, the sampling window length of the dFC stream. However, it is convenient to pool speed samples into a few histograms, with close enough τ to return statistically indistinguishable distributions. There are no rules for choosing the window sizes to pool together, they are a matter of arbitrary choice.

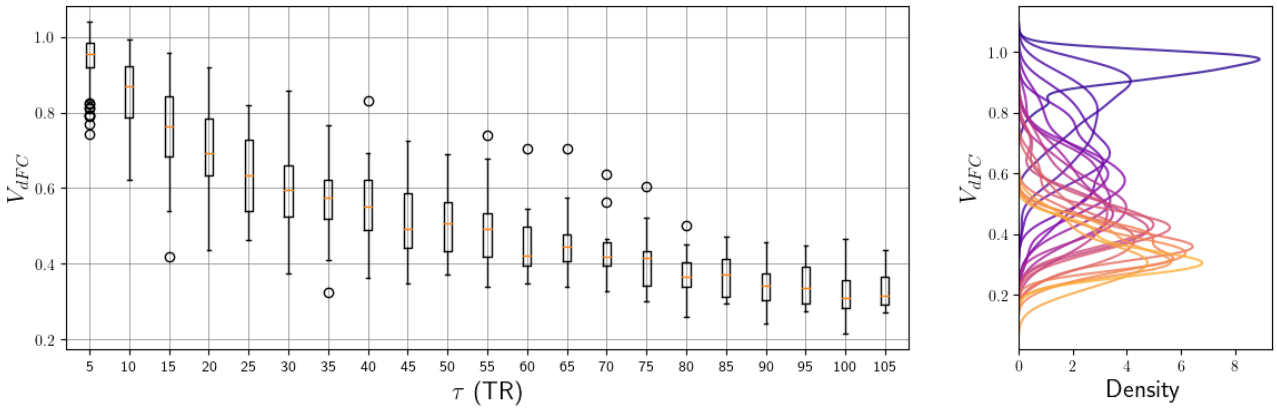

Figure 3.1: Global speed dependence on τ. On the left, every boxplot shows the first quartile, third quartile, median, and flier points of the V_{dFC} distribution for a given τ in a single subject. On the right, the heights of the corresponding normalized kernel density estimations provide a graphical visualization of the relationship between the mean and the standard deviation of every speed distribution.

For the sake of comparison, we decided to form three histograms, corresponding to the same window length ranges (in seconds) used by Battaglia et al. [11]. Due to the different repetition time (TR) in our study compared to Battaglia et al. [11], this choice yields different ranges in terms of the number of frames.

Short range $\sim 6\text{s} < \tau <\sim 15\text{s}$ $(8 - 20\text{TRs})$

Mid range $\sim 15\text{s} < \tau <\sim 60\text{s}$ $(21 - 82\text{TRs})$

Long range $\sim 60\text{s} < \tau <\sim 210\text{s}$ $(83 - 290\text{TRs})$

The aim of this work is not to characterize individual differences, so no distinction has been made across datasets of different subjects. This approach is equivalent to considering the global speed of some sort of *average subject*. So, besides the pooling process within different streams of the same realization, we merged the histograms of all the different participants. In so doing, we lost possible

differences that could derive from demographic factors such as age or sex. This could be a limitation in the case of unbalanced classes.
All sessions have the same temporal length so they are comparable.

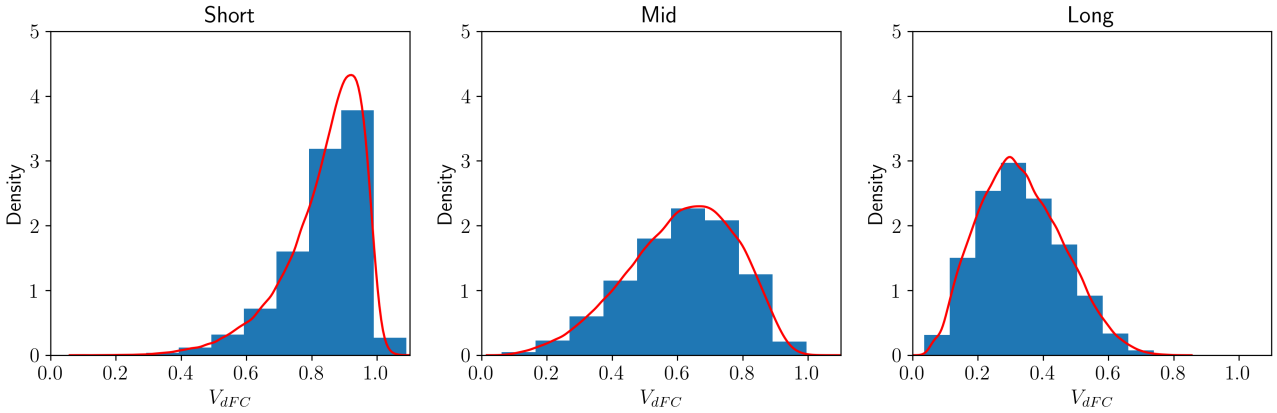

Figure 3.2: Comparison of the distribution of the instantaneous global speed V_{dFC} pooled over the three distinct window-size ranges and merged across subjects. The plot shows the empirical histograms and kernel density estimations for each range.

Figure 3.2 reports the results of this analysis. The global dFC speed distributions have a clear peak (i.e. *typical dFC*) around the median value. These distributions deviate from Gaussianity for each range (Lilliefors test with $p < 0.05$). This can be interpreted as a partial proof of the complex behavior over different temporal scales. The excess kurtosis it's negative (≈ -0.3) for both mid and long ranges, while the short range appears to be leptokurtic (excess kurtosis of ≈ 1.8). The fat tails indicate that FC reconfiguration events of anomalous rapidity are observed with relatively large probability in the short temporal scale.
The so-defined speed of reconfiguration slows down when the window size τ is increased. This can be interpreted as the result of a stochastic exploration of the space of possible configurations which tends to stabilize itself in longer ranges (so with more aggregated information).

3.2 MINDy behaviors

To fit the MINDy model to the data, we used the MATLAB function *MINDy_Simple* via Matthew F. Singh's GitHub page. This function returns the phenomenological parameters of the model: the weights W, the curvature α, and the decay diagonal matrix D. We fitted the model to every single subject in order to obtain personalized parameters that could reproduce individual differences in brain dynamics.

We used the explicit Euler's method to integrate the ordinary differential equation that characterized the model and reproduce the BOLD times series for each brain region and in each participant.

$$x_{t+\Delta t} = x_t + (W\psi_\alpha(x_t) - Dx_t + \varepsilon_t)\Delta t$$

We used the temporal resolution $\Delta T = \text{TR}$ and a process Gaussian noise ε_t, uncorrelated between parcels, at each time step. The noise depends on the standard deviation σ_ε, whose role will be investigated afterward.

Two behaviors

Once fitted the model to the datasets and numerically integrated the dynamics, two different behaviors in the obtained BOLD signals emerged.
Even for $\sigma_\varepsilon = 0$, simulations of some subjects exhibit a periodic cycle and non-trivial dynamics, while simulations from others converge to fixed values.

In figure 3.3 we display the differences in the datasets whose dynamics exhibit a limit cycle and whose simulated BOLD signals converge to a fixed point. In the first column, we report the behavior for $\sigma_\epsilon = 0$, so when no noise is added. After some iterations of the explicit Euler's method, the integrated dynamics converge from the random initial point to one of the two behaviors described before.

For large enough noise, the dynamic is "activated" in both cases and the model better succeeds in reproducing the functional connectivity of the whole session. So, both behaviors can correctly reproduce the static rsFC when a proper σ_ε is used (see the specific subsection). However, models converging to a fixed point completely fail to reproduce the observed dynamic functional connectivity and are not able to return the right distribution of the global speed.

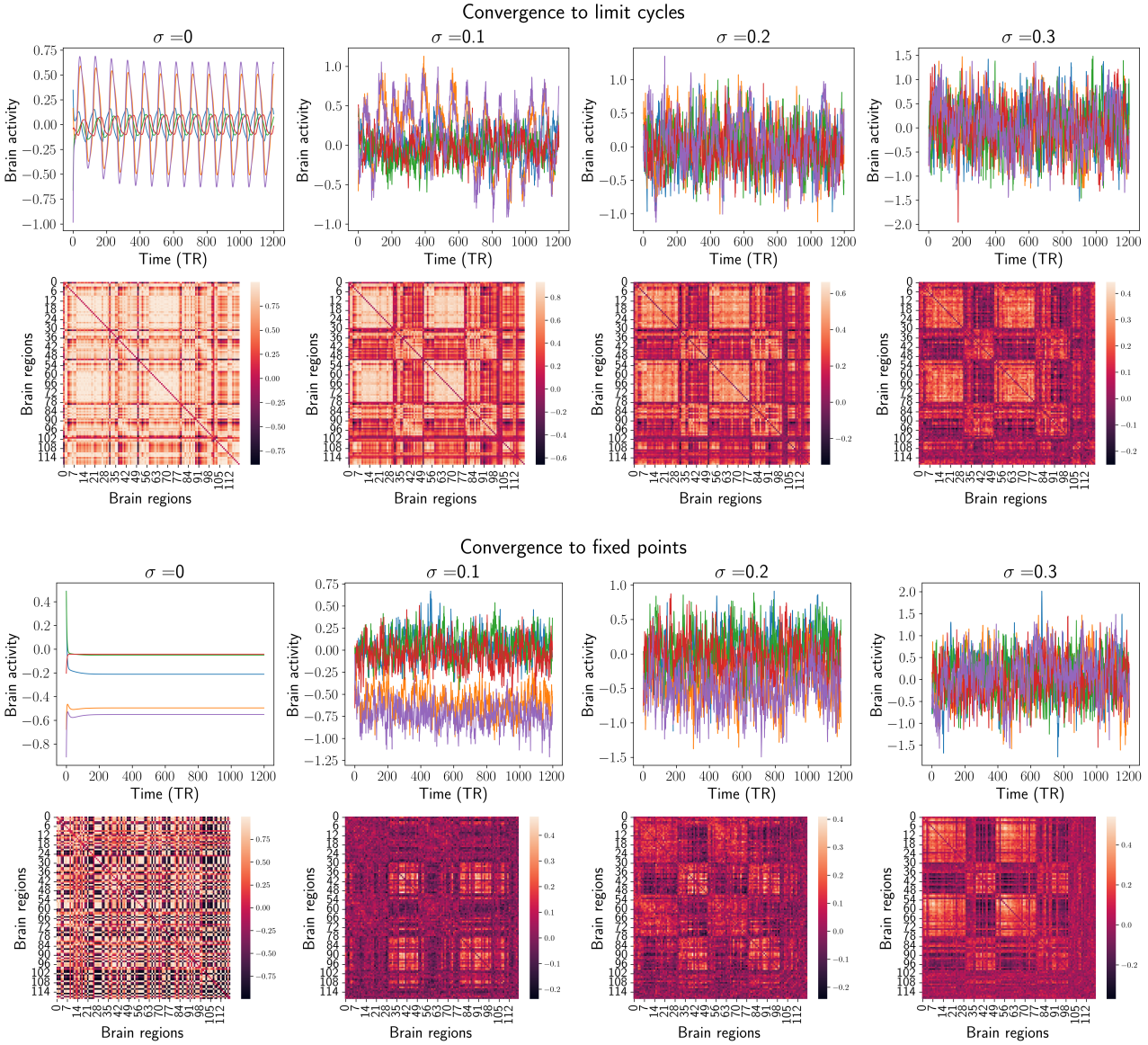

Figure 3.3: Comparison of the two behaviors in terms of simulated BOLD signals and static FC. Each column shows examples of the results of the MINDy model integration for a given σ_ε. The showed signals are just 5 random time series from the 119 available.

Role of sigma in static FC

In the following paragraph we will discuss the role played by the standard deviation σ_ε of the Gaussian noise for what concerns the static FC. It can be treated as a hyperparameter of the model.

As shown in figure 3.4, it is necessary to use a proper σ_ε to successfully obtain the simulated functional connectivity. This was tested by computing the Pearson correlation between the entries of the FC matrix from the fMRI session and the simulated one. This metric of performance was treated as a function of σ_ε for each subject (on the left).

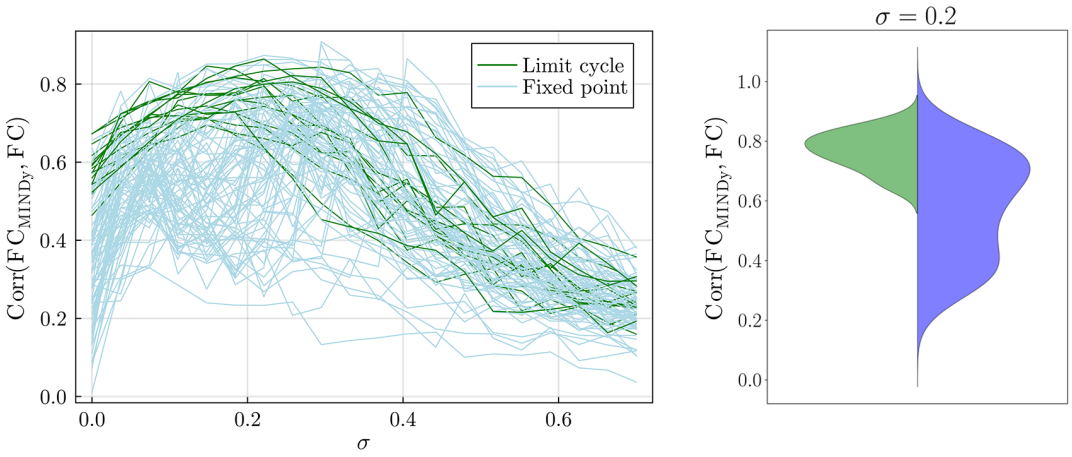

Figure 3.4: Full session FC and sigma. On the left, for each subject, the correlation between the FC obtained from the data and the simulated one as a function of the σ_ε. It is a measure of model performance. On the right, the violin plot of the correlation for $\sigma_\varepsilon = 0.2$ for both behaviors: limit cycle (green) and fixed point (blue).

There are differences in the performance of the model between the two behaviors or classes of convergence. Lower performances are obtained for subjects whose simulated time series converge to a fixed point in the absence of noise.
Both too-small and too-large values of σ_ε fail to reproduce the FC. Thus, as expected, adding some noise is needed but it must not dominate the dynamics.
The greatest performances are obtained for σ_ε approximately between 0.1 and 0.3. To analyze the dynamics (section 3.3) we will use $\sigma_\varepsilon = 0.2$ but the results are robust to small changes of this hyperparameter. In figure 3.4, on the right, the corresponding model performances are shown in a violin plot for both classes. It is important to note the large variance of these in case of convergence to a fixed point.

Relationship with parameters

The MINDy fitting procedure returns three phenomenological parameters (α, D, and W) which tune the dynamics. Each participant has its own set of parameters. It is interesting to study whether or not they play a role in the distinction between the two behaviors.

To test this hypothesis, we defined a measure of distance between the distributions of the same parameter evaluated for different subjects. This metric has been computed between different participants within the same class of behavior (limit cycle and fixed point) and across classes.
Because the sample of subjects that exhibit convergence to a fixed point is larger, it has been downsampled to the same size as the other to avoid distortions in the results.

Parameters α and D are both vectors with lengths equal to the number of the considered neural populations (the parcels defined by the chosen brain atlas). We chose to compute the Euclidean distance between pairs of vectors. On the other hand, the weights W are matrices. To quantify the similarity between them we used the Euclidean distance between pairs of flatten matrices.

If parameter values helped to differentiate between the two classes, we would expect greater distances across classes rather than within the same class. That would be equivalent to saying that parameters values leading to the same dynamical behavior are more likely to be similar.
The results are reported in figure 3.5. Among all parameters, the non-linearity of the model, which is

controlled by the parameter α, appears to play a role in characterizing the classes. The convergence to a limit cycle seems to be related to more uniform values of α, compared to convergence to a fixed point. However, the distributions of α are very similar for the two classes: the mean value of α is 5.054 in the case of limit cycles (16 subjects), against 5.061 otherwise (80 subjects randomly downsampled to 16). The standard deviations are 0.047 against 0.052. HWe think that a more reliable statistical analysis to probe the effect of α (if any exists) would require a larger sample.

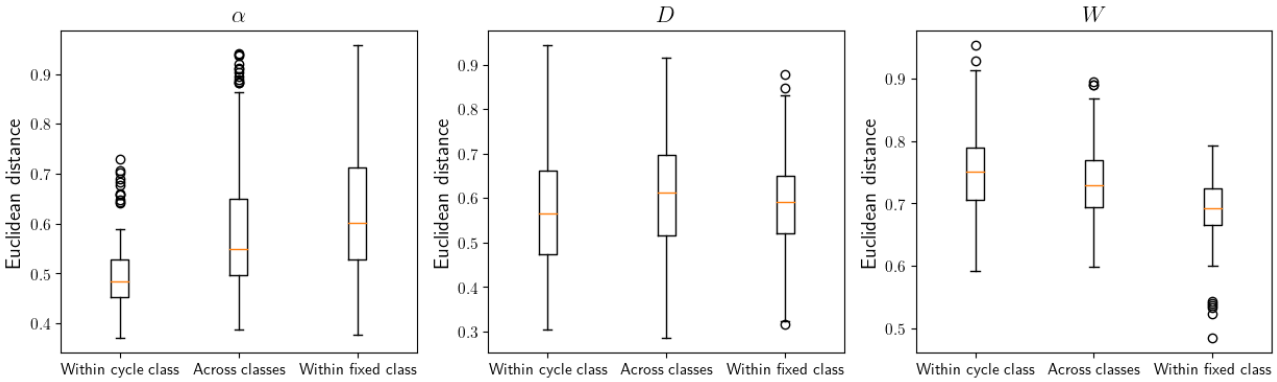

Figure 3.5: Distances between pairs of sets of parameters within the same class (limit cycle and fixed point) and across classes. It has been used the Euclidean distance between pairs of α and D vectors and between pairs of W flatten matrices.

Linearized model

MINDy is nonlinear due to the definition of the transfer function ψ_α. However, this does not inherently imply that the obtained dynamics are not trivial and differ from models working in linear approximation.

Important information about the model dynamics can be obtained by evaluating the linearized system and its eigenvalues. The first order differential equation which defined the model is:

$$\dot{x}_t = W\psi_\alpha(x_t) - Dx_t + \varepsilon_t$$

where ψ_α is defined as:

$$\psi_\alpha(x_t) = \sqrt{\alpha^2 + (bx_t + 0.5)^2} - \sqrt{\alpha^2 + (bx_t - 0.5)^2}$$

and whose derivative is:

$$\frac{\partial \psi_\alpha}{\partial x_t}(x_t) = \frac{b(bx_t + 0.5)}{\sqrt{\alpha^2 + (bx_t + 0.5)^2}} - \frac{b(bx_t - 0.5)}{\sqrt{\alpha^2 + (bx_t - 0.5)^2}}$$

More precisely, ψ_α is a function $\mathbb{R}^N \to \mathbb{R}^N$ (where N is the number of brain parcels) whose entries $\psi_{\alpha,1}, \psi_{\alpha,2}, ..., \psi_{\alpha,N}$ depend only on the corresponding value $x_{t,1}, x_{t,2}, ..., x_{t,N}$. The value $x_{t,i}$ quantifies the activity of the neural population i at time t. So, its jacobian is diagonal:

$$J_\psi(x_t) = \text{diag}\left(\frac{\partial \psi_\alpha}{\partial x_{t,1}}(x_{t,1}), \frac{\partial \psi_\alpha}{\partial x_{t,2}}(x_{t,2}), \quad ... \quad , \frac{\partial \psi_\alpha}{\partial x_{t,N}}(x_{t,N})\right)$$

The systems can be then linearized around an equilibrium $\tilde{x} \in \mathbb{R}^N$:

$$\dot{x}_t \approx \tilde{A} \cdot x_t \quad \text{where } \tilde{A} = W \cdot J_\psi(\tilde{x}) - D$$

Upon completion of the fitting procedure of every dataset, each set of parameters was used to compute the eigenvalues λ around an equilibrium. We can rule out the hypothesis of trivial dynamics (i.e.,

convergence to a global stable fixed point attractor) by examining the eigenvalues of the linearized system at zero. The origin is of course an equilibrium point, corresponding to null activity. Since all subjects have at least one eigenvalue with positive real part, we can conclude, according to the analysis reported in [16], that no equilibrium point is globally stable. In fact, the transfer function is odd ($\psi(-x) = -\psi(x)$) thus if any $x_s \neq 0$ is a fixed point, so is its reflection $-x_s$. If x_s is stable and thus possesses an attractive basin V of non-zero measure, then $-V$ is the attractive basin of $-x_s$, and therefore x_s is not a global equilibrium. Moreover, the origin cannot be stable because there is at least one eigenvalue with positive real part. It follows that any fixed point is not globally stable but unstable or not unique.

The two behaviors can be described and better characterized in terms of the eigenvalues λ of the linearized model around an equilibrium point of the corresponding dynamics. In case of convergence to a fixed point, $\tilde{x}$ was set to be equal to the array of values of the stabilized activity. Otherwise, the system was linearized around the origin, since the periodic oscillations are centered in zero. This procedure does clearly not provide a classification method, but eigenvalues of the linearized dynamics can be useful to better understand the dynamics.
Another valuable tool to visualize the differences between the two behaviors is the phase portrait of the subjects, so the simulated time series were projected onto the first 3 principal components. This was implemented with the *sklearn.decomposition.PCA* function.

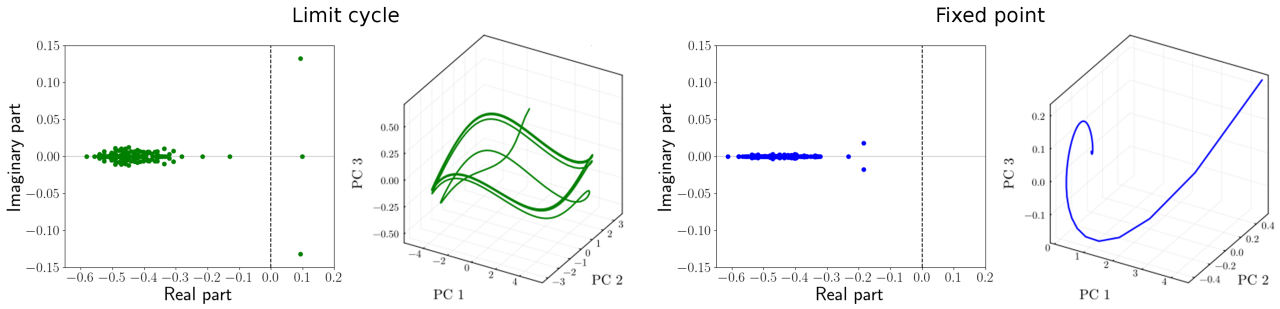

Figure 3.6: Comparison of the two behaviors in terms of eigenvalues λ of the linearized system around the corresponding equilibrium, and phase portrait of the two behaviors. For both classes of behavior, we show examples of the set of eigenvalues and the projection of the simulated time series onto the first 3 principal components. In the case of a limit cycle, periodic orbits link neighborhoods of two unstable fixed points. Otherwise, the systems converge to a single point.

The datasets whose obtained dynamics converge to a fixed point have only eigenvalues with negative real parts, as follows from the theory of dynamical systems. An important role is played by the maximum (real part) eigenvalue, whose magnitude characterizes how fast the dynamics reach the equilibrium.
Figure 3.7 describes the relationship between the maximum eigenvalue of each subject and the number of points before the convergence, quantified as the number of Euler's iterations until the difference between a pair of successive points was lower than a chosen threshold. The speed of convergence is the same for every time series, as the dynamics are dominated by the maximum eigenvalue. As expected, the characteristic time of the exponentially fast convergence is proportional to the reciprocal of that eigenvalue.
On the other hand, in the case of a limit cycle, there is a correlation between the maximum eigenvalue of the linearized system in the origin and the period of the cycle, as obtained through the *fast Fourier transform* (*numpy.fft.fft*). Moreover, the scatterplots of the eigenvalues in the complex plane suggest that the eigenvalues with positive real parts have also the greatest imaginary components. As the imaginary components are related to the period of an (unstable) oscillation around zero, this suggests that such unstable oscillation is stabilized by non-linear terms in the equation, leading to a stable limit cycle.

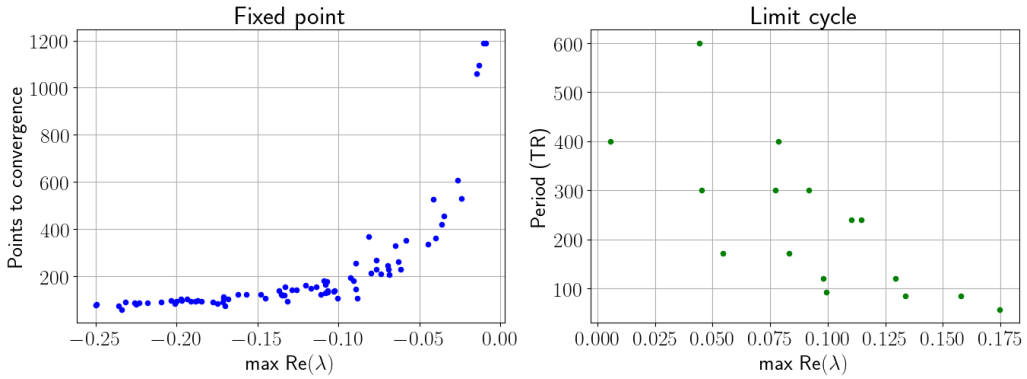

Figure 3.7: Relationship between the maximum eigenvalue of the linearized system and the dynamics for $\sigma_\varepsilon = 0$. On the left, the number of iterations needed to converge to the fixed points. On the right, the period of the limit cycles. Each dot represents a subject.

3.3 MINDy and dFC

The MINDy model is able to reproduce the functional connectivity of the whole session (as described before), which is a static feature of the fMRI time series. The performances are better in the case of convergence to a limit cycle. Moreover, MINDy is able to predict the activity over very short timescales, comparable to one integration step [15]. This is substantially different from understanding whether or not this model can predict the actual dynamics of brain activity, which is characterized by more slowly fluctuating temporal patterns.
Singh et al. [15] successfully tested the model accuracy in capturing longer-term dynamic patterns using the *Dynamic Conditional Correlation* (DCC) method and comparing the standard deviation of the conditional correlation time series with the actual data.
In the following paragraphs, we will discuss the performances of the MINDy model in reproducing the observed distribution of the global dFC speed V, and the relationship between model performance and the two behaviors described in section 3.2. The experimental distributions for the three window length ranges were described in section 3.1.

Using $\sigma_\varepsilon = 0.2$, we computed the pooled V distribution for each range merging all the subjects within the same class (figure 3.8). The results are quite unsatisfactory. As evaluated in this aggregate form, datasets whose dynamics converge to a fixed point completely fail to reproduce the experimental behavior. The performances are better in the case of limit cycle, but, even in this case, models are far from matching the empirical distribution of the global speed.

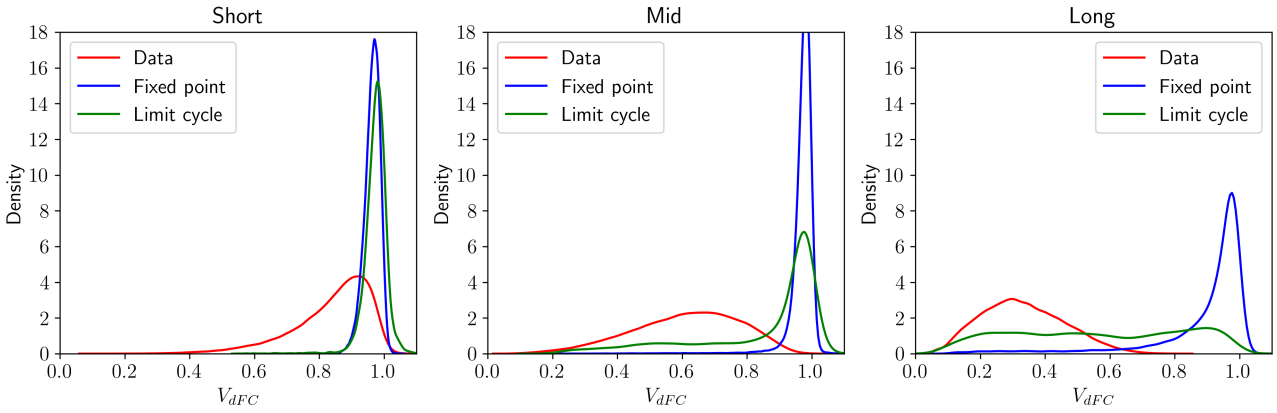

Figure 3.8: Comparison between the distributions (kernel density estimations) obtained by MINDy and the experimental one. The simulations were computed with $\sigma_\varepsilon = 0.2$.

We tested the agreement between the actual dFC speed distributions and the ones obtained by MINDy and its dependence on the magnitude of the noise (the standard deviation σ_ε). The distances were quantified by the two-sided Kolmogorov–Smirnov statistics for each range (short, mid, long), implemented by the *scipy.stats.kstest* function. Note that, unlike in figure 3.4 (role of sigma in static FC), this is the opposite of a measure of performance. The results are shown in figure 3.9.

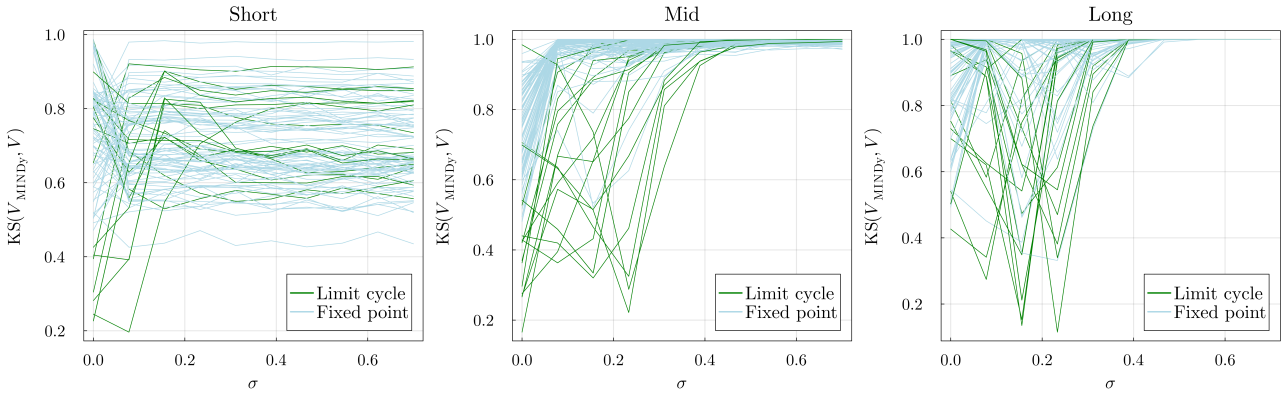

Figure 3.9: For each range, two-sided Kolmogorov–Smirnov distances between the actual dFC speed distributions and the ones obtained by MINDy. The distances, treated as a function of the noise magnitude σ_ε, provide information about the model performances. This plot also highlights the differences between the two behaviors: convergence to a limit cycle (green) and to a fixed point (blue).

For the short-range, distances, treated as a function of σ_ε, quickly converge to a fixed value. This value is different for each subject and it is maintained also for large σ_ε. The actual distributions for this range peaked at 1 (figure 3.2), which is also the average value obtained for dynamics dominated by Gaussian noise. Indeed, a set of completely random time series corresponds to a Gaussian dFC speed profile peaked at 1. Thus, the short-range distances for large σ_ε represent a measure of the overlap between the ground truth histogram of each subject and the distribution obtained for random behavior, rather than the actual performances of the model.
In both the mid and the long ranges there are significantly different performances for the two classes of behavior. In the case of convergence to a fixed point, the distances quickly increase from the value obtained for $\sigma_\varepsilon = 0$ to 1. The model is therefore not able to reproduce the correct speed of reconfiguration. The initial points are interesting because they represent some changes in the FC states also for apparently flat time series. This is because the time series keep small oscillations anyway, exponentially smaller at each iteration of the integration method. Removed the initial burn-in period, these residual fluctuations have a very small magnitude, but Pearson's correlation, on which the speed is defined, is normalized by the standard deviations. Thus, the functional connectivity is still defined but problems may occur due to the round-off precision.
In the case of a limit cycle instead, there are better performances (lower Kolmogorov–Smirnov distances) when some noise is used. The best performances are again obtained for σ_ε approximately between 0.1 and 0.3, similar to what happened with the static functional connectivity (figure 3.4). However, the model cannot be declared successful as the distances remain relatively large.

Figure 3.10 describes the relationship between the eigenvalues of the linearized systems (obtained for each class as described before) and the Kolmogorov–Smirnov statistics. Similarly to what did in the static case, we used $\sigma_\varepsilon = 0.2$ to simulate the BOLD time series.
This analysis confirms the failure of the model in the case of convergence to a fixed value, with few exceptions that were lost in the aggregate analysis (especially in the long-range). In the case of convergence to a limit cycle, the plot shows the relationship between the maximum eigenvalue and the performance of the model. Since the eigenvalues are negatively correlated with the period of the simulated time series, the greatest performances are obtained with the shortest periods.

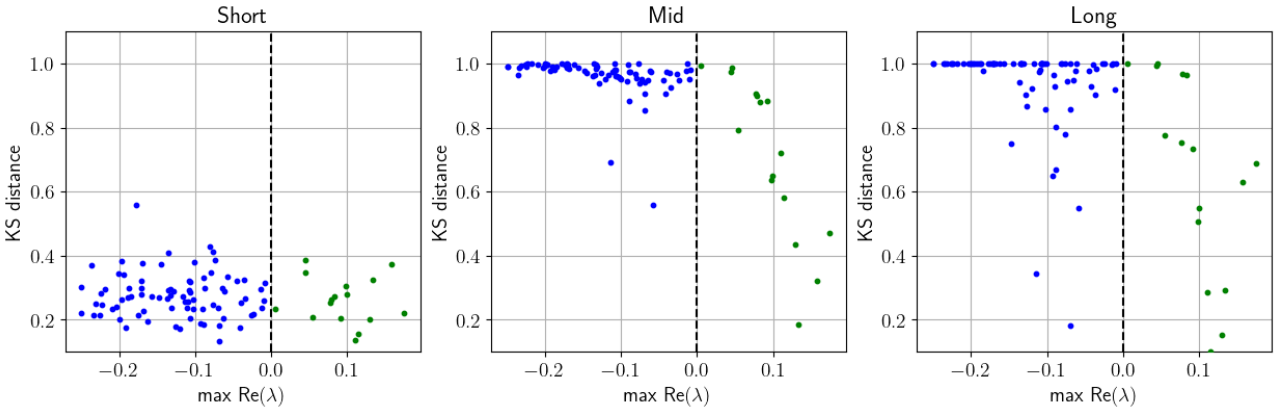

Figure 3.10: Relationship between the maximum (real part) eigenvalue and the two-sided Kolmogorov–Smirnov test between the experimental dFC speed distributions and the obtained ones for $\sigma_\varepsilon = 0.2$. Each dot is a subject.

Detrended fluctuation analysis

Detrended fluctuation analysis (DFA) is a powerful statistical method to detect intrinsic self-similarity and long-range persistence in a time series [11,17]. The resulting coefficient α_{DFA} (not to be confused with the MINDy parameter) characterizes the self-correlation of long-memory processes.

Given a time series of N discrete elements $x_1, x_2, ..., x_N$, to perform the DFA we need to convert it into an unbounded process via the cumulative sum of its elements:

$$X(t) = \sum_{i=1}^{t} (x_i - < x >)$$

where $< x >$ is the mean of the time series. The subtraction of the mean eliminates the global trend of the signal.
The time series is then split into M non-overlapping segments $q = 1, ..., M$ of fixed length k each. For each segment q the squared fluctuation $F_q^2(k)$ was computed as the mean squared difference between $X(t)$ and its local trend $Y_q(t)$. In the linear case, $Y_q(t)$ is the regression line of $X(t)$ over the time interval of the segment q.

$$F_q^2(k) = \frac{1}{k} \sum_{t=qk+1}^{qk+k} (X(t) - Y_q(t))^2$$

We define the fluctuation strength $F(k)$ as the average $F_q(k)$ over the identically sized segments $q = 1, ..., M$. The fluctuation strength is treated as a function of the length k.
We compute $F(k)$ for a set of K different lengths $k_1 \approx 4 < k_2 < ... < k_K \approx N$, roughly equally spaced on a logarithmic scale (geometric progression). Then, $F(k)$ is fitted with the linear power law:

$$\log F(k) = \alpha_{DFA} \log k + C$$

The obtained α_{DFA} is a generalization of the Hurst exponent, leading to the following interpretation:

- $0 < \alpha_{DFA} < 0.5$: the process (time series) has a memory and exhibits anti-correlation.
- $\alpha = 0.5$: the process is indistinguishable from a random process with no memory. It displays uncorrelated Gaussian fluctuations ("white noise").
- $0.5 < \alpha_{DFA} < 1$: the process has a memory, and it exhibits positive correlations.
- $\alpha_{DFA} > 1$: the process is non-stationary.

We performed the analysis both on the experimental time series and on the surrogate time series. Figure 3.11 reports some of the obtained results.
For all the subjects, the mean α_{DFA}, averaged on the set of time series, is approximately between 0.55 and 0.80. The experimental datasets whose obtained MINDy dynamics converge to a limit cycle seem to be characterized by slightly lower α_{DFA} values. This can be observed in the kernel density estimation on top of the left figure (3.11). Moreover, the self-correlation seems to be unrelated to the model non-linearity.
The plot on the right shows some negative correlation ($r = -0.4$) between the obtained maximum eigenvalue (characterizing the model behaviors) and the experimental self-correlation. However, a more robust analysis definitely requires more data and more balanced classes.
The MINDy model tends to overestimate and amplify the self-correlations in the data. The performances are qualitatively good for the subjects with lower eigenvalues, but they rapidly get worse.

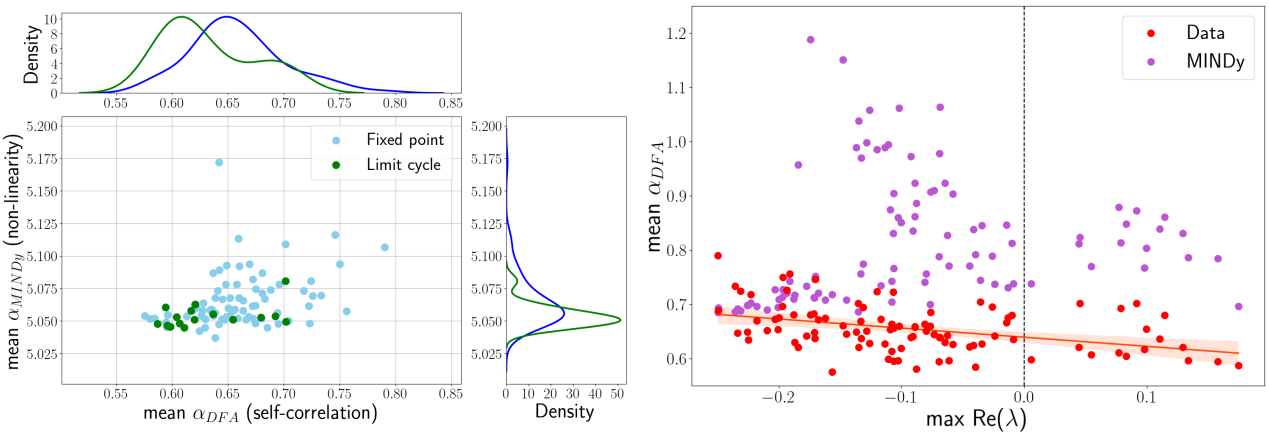

Figure 3.11: On the left, the relationship between the self-correlation (α_{DFA}) and the obtained MINDy non-linearity (α_{MINDy}). Each dot corresponds to a single subject and reports the average α_{DFA} and α_{MINDy} from the 119 experimental and surrogate time series, respectively. The plot shows also the distributions of these two features, both for the fixed point and limit cycle classes. On the right, the relationship between the obtained max (real part) eigenvalues of the linearized systems and α_{DFA}, both computed for the actual and simulated time series. The differences between red and purple dots are a measure of the performances of the model ($\sigma_\varepsilon = 0.2$) in reproducing the corrected α_{DFA}.

Chapter 4

Conclusions

In this work, we studied whether and how a particular generative causal model (called Mesoscale Individualized Neurodynamic, MINDy) can reproduce a scalar feature of the time series from functional magnetic resonance imaging, the global dynamic functional connectivity speed.

We fitted the model to real datasets (from the Human Connectome Project) and numerically integrated the dynamics with no added noise. Then, we studied the role of the magnitude of the Gaussian noise in both static and dynamic functional connectivity.
We noticed that two different behaviors emerged in the surrogate BOLD signals: in some cases (fixed points), the dynamics converge to a stable equilibrium; in other cases (limit cycles), the dynamics exhibit periodic orbits that link neighborhoods of unstable fixed points in the phase portrait. Both classes can reproduce the static resting state functional connectivity, but the models converging to a fixed point fail to return the right distribution of the global speed. The performances increase if the dynamics converge to a limit cycle, but the model cannot be declared completely successful as the distances from the ground truth remain relatively large.
The maximum (real part) eigenvalue of the linearized system, when computed around the correspondent equilibrium, plays an important role. It correlates with the performances of the model in the case of limit cycles and it seems to be related to the self-correlation of the experimental time series.

The main limitation of this work is the fitting procedure, made by the most basic MINDy high-level function. It could be interesting to better investigate the fitting preprocessing (deconvolution/filtering) and the role of the hemodynamic response functions. Also, more precise and robust analyses require more data, especially for what concerns the limit cycles. Finally, a more thorough dynamical analysis would be required to understand i) how model parameters determine the dynamical behavior ii) what features of the simulated time series make them unsuitable to correctly reproduce the observed dynamical functional connectivity speed.

Bibliography

[1] Elena A. Allen, Eswar Damaraju, Sergey M. Plis, Erik B. Erhardt, Tom Eichele, and Vince D. Calhoun. Tracking Whole-Brain Connectivity Dynamics in the Resting State. *Cerebral Cortex*, 24(3):663–676, 11 2012.

[2] Enzo Tagliazucchi, Frederic Von Wegner, Astrid Morzelewski, Verena Brodbeck, and Helmut Laufs. Dynamic bold functional connectivity in humans and its electrophysiological correlates. *Frontiers in Human Neuroscience*, 6, 2012.

[3] Raphaël Liégeois, Timothy O. Laumann, Abraham Z. Snyder, Juan Zhou, and B.T. Thomas Yeo. Interpreting temporal fluctuations in resting-state functional connectivity mri. *NeuroImage*, 163:437–455, 2017.

[4] Timothy O. Laumann, Abraham Z. Snyder, Anish Mitra, Evan M. Gordon, Caterina Gratton, Babatunde Adeyemo, Adrian W. Gilmore, Steven M. Nelson, Jeff J. Berg, Deanna J. Greene, John E. McCarthy, Enzo Tagliazucchi, Helmut Laufs, Bradley L. Schlaggar, Nico U. F. Dosenbach, and Steven E. Petersen. On the Stability of BOLD fMRI Correlations. *Cerebral Cortex*, 27(10):4719–4732, 09 2016.

[5] Catie Chang, David A. Leopold, Marieke Louise Schölvinck, Hendrik Mandelkow, Dante Picchioni, Xiao Liu, Frank Q. Ye, Janita N. Turchi, and Jeff H. Duyn. Tracking brain arousal fluctuations with fmri. *Proceedings of the National Academy of Sciences*, 113(16):4518–4523, 2016.

[6] David C Van Essen, Stephen M Smith, Deanna M Barch, Timothy EJ Behrens, Essa Yacoub, Kamil Ugurbil, Wu-Minn HCP Consortium, et al. The wu-minn human connectome project: an overview. *Neuroimage*, 80:62–79, 2013.

[7] Matthew F Glasser, Stamatios N Sotiropoulos, J Anthony Wilson, Timothy S Coalson, Bruce Fischl, Jesper L Andersson, Junqian Xu, Saad Jbabdi, Matthew Webster, Jonathan R Polimeni, et al. The minimal preprocessing pipelines for the human connectome project. *Neuroimage*, 80:105–124, 2013.

[8] Alexander Schaefer, Ru Kong, Evan M Gordon, Timothy O Laumann, Xi-Nian Zuo, Avram J Holmes, Simon B Eickhoff, and BT Thomas Yeo. Local-global parcellation of the human cerebral cortex from intrinsic functional connectivity mri. *Cerebral cortex*, 28(9):3095–3114, 2018.

[9] Bruce Fischl, David H Salat, Evelina Busa, Marilyn Albert, Megan Dieterich, Christian Haselgrove, Andre Van Der Kouwe, Ron Killiany, David Kennedy, Shuna Klaveness, et al. Whole brain segmentation: automated labeling of neuroanatomical structures in the human brain. *Neuron*, 33(3):341–355, 2002.

[10] Bruce Fischl. Freesurfer. *Neuroimage*, 62(2):774–781, 2012.

[11] Demian Battaglia, Thomas Boudou, Enrique C.A. Hansen, Diego Lombardo, Sabrina Chettouf, Andreas Daffertshofer, Anthony R. McIntosh, Joelle Zimmermann, Petra Ritter, and Viktor Jirsa. Dynamic functional connectivity between order and randomness and its evolution across the human adult lifespan. *NeuroImage*, 222:117156, 2020.

[12] Lucas M. Arbabyazd, Diego Lombardo, Olivier Blin, Mira Didic, Demian Battaglia, and Viktor Jirsa. Dynamic functional connectivity as a complex random walk: Definitions and the dfcwalk toolbox. *MethodsX*, 7:101168, 2020.

[13] Nora Leonardi and Dimitri Van De Ville. On spurious and real fluctuations of dynamic functional connectivity during rest. *NeuroImage*, 104:430–436, 2015.

[14] Diego Lombardo, Catherine Cassé-Perrot, Jean-Philippe Ranjeva, Arnaud Le Troter, Maxime Guye, Jonathan Wirsich, Pierre Payoux, David Bartrés-Faz, Régis Bordet, Jill C. Richardson, Olivier Felician, Viktor Jirsa, Olivier Blin, Mira Didic, and Demian Battaglia. Modular slowing of resting-state dynamic functional connectivity as a marker of cognitive dysfunction induced by sleep deprivation. *NeuroImage*, 222:117155, 2020.

[15] Matthew F. Singh, Todd S. Braver, Michael W. Cole, and ShiNung Ching. Estimation and validation of individualized dynamic brain models with resting state fmri. *NeuroImage*, 221:117046, 2020.

[16] Matthew F. Singh. Relating spontaneous activity and cognitive states via neurodynamic modeling. *Arts Sciences Electronic Theses and Dissertations*, 2346, 2021.

[17] Richard Hardstone, Simon-Shlomo Poil, Giuseppina Schiavone, Rick Jansen, Vadim V Nikulin, Huibert D Mansvelder, and Klaus Linkenkaer-Hansen. Detrended fluctuation analysis: a scale-free view on neuronal oscillations. *Front. Physiol.*, 3:450, November 2012.